12 Determination of the mass scale

12.1 Introduction

This chapter describes some of the methods which will be used to understand to the best possible accuracy the absolute measurement scale of the ATLAS detector when the experimental data will be used to extract precise estimates of the masses of known or newly discovered particles.

The need for accurate experimental measurements of particle masses does not require much justification, given the progress made in particle physics over the past decades through such measurements. Nevertheless, a few examples of what might be achieved with ATLAS at the LHC are listed below and described in more detail in the relevant chapters devoted to the physics performance.

An accurate measurement of the Higgs boson mass will provide strong additional constraints on the underlying model. A statistical accuracy of ~0.1% can be achieved over a wide range of Higgs boson masses (see Sections 19.2.12.1 and 19.3.4), and the power of a constraint at this level is clearly demonstrated in the context of the global fits to the parameters of minimal supergravity models, as described in Section 20.2.9.

If supersymmetry were to be discovered at the LHC, it has been demonstrated already a few years ago that ATLAS would be able to perform a wide set of precision measurements of various supersymmetric particle masses (see Chapter 20). The more accurate these measurements will be, the tighter the constraints on the fundamental parameters of the underlying SUSY model will be (see Sections 20.2.9, 20.2.10 and 20.3.5).

Very precise measurements of the masses of the W boson (see Section 16.1) and of the top quark (see Section 18.1.3), beyond those which will be achieved at the Tevatron and at LEP2 in the near future, will provide further additional constraints on the Standard Model. If a Standard Model Higgs boson were also to be discovered at the LHC, the combination of all these measurements would provide overall constraints of the Standard Model an order of magnitude stronger than those available today.

The physics goals described above have led to the following requirements for the knowledge of the absolute scale of energy and momentum measurements in ATLAS:

- In the case of electrons and muons, the scale should be known to an accuracy of ~0.1%. A similar accuracy has already been reached by the CDF [12-1] and D0 [12-2] experiments at the Tevatron. This accuracy should be achievable, given that ATLAS will be able to benefit directly from much larger statistics of vector boson leptonic decays. This will however require considerable work.

  This accuracy will be adequate for almost all the physics goals of ATLAS at the LHC, but will be needed over the full lifetime of the experiment and in particular at the highest luminosities. The one exception is the measurement of the W mass at low luminosity, which requires a much better knowledge of the measurement scale of electrons and muons, namely at the level of 0.02%, as explained in more detail in Section 16.1.4.

- In the case of hadronic jets, the scale should be known to an accuracy of ~1%. In principle, it would be desirable to measure decays involving quarks with a similar accuracy to those

involving leptons. However, it is clear that the fragmentation and hadronisation of the original partons lead to uncertainties in the experimental measurements, which cannot be readily decreased below this level of 1%.

Another aspect linked to the understanding of the absolute scale of measurements performed using the ATLAS detector concerns calorimeter energy measurements at a scale of the order of a TeV or more, which cannot be constrained directly from data taken in test beams during the detector construction. The physics topics of interest in this area are:

- for the EM Calorimeter scale, mass measurements of possible new vector bosons decaying into electrons (see Section 21.6.1);
- for the hadronic calorimetry, QCD physics with high-p_T hadronic jets (see Section 15.5), mass measurements of leptoquarks decaying to a lepton and a jet (see Section 21.4), and quark compositeness studies (see Section 21.5.1).

None of the above physics studies requires an understanding of the absolute scale of the energy measurements to a very high level of accuracy. However, departures of the calorimeter response from linearity may cause serious problems in the searches for quark compositeness using the jet p_T spectrum, and these are discussed in some detail in Sections 9.1.1.3 and 21.5. Therefore this chapter will only discuss issues concerning the overall mass scale in ATLAS.

In order to understand the magnitude of the task set by the physics goals described above, it is important to recall that, when the first LHC collisions will be recorded in the detector, the knowledge of the absolute calibration of the various systems in ATLAS prior to data-taking will be far from that ultimately required:

- the absolute momentum scales for charged particles measured in the Inner Detector and the Muon System will be known to 0.5% or better from the initial magnetic field maps and geometrical surveys;
- the absolute energy scale for electrons and photons will be known to 1-2% from the transfer to the experiment of calibration data taken with electrons in test beam;
- the absolute energy scale for hadronic jets over $|\eta| < 3.2$ will be known to ~5-10% from the transfer to the experiment of calibration data taken with charged pions in test beam and from Monte Carlo simulations of jet fragmentation into hadrons.

There would be clearly little hope to improve this initial knowledge by a factor of ~25 for electrons and muons and by a factor of ~5-10 for hadronic jets, if the large production cross-sections expected for known resonances ($Z \rightarrow ee$, $Z \rightarrow \mu\mu$ and $W \rightarrow jj$) were not to allow very precise and high-statistics *in situ* calibration procedures to be used. The Z line shape will be known to an accuracy of better than 10^{-4} at the LHC, and the W mass will be known to an accuracy of ~5×10^{-4}. These accuracies are significantly better than the ones required to set the absolute scale, respectively for electrons and muons using $Z \rightarrow ee$ and $Z \rightarrow \mu\mu$ decays and for jets using $W \rightarrow jj$ decays.

The abundant production of vector bosons at the LHC will be used to set the absolute scale at the right value to a very high accuracy. Nevertheless, care will have to be taken to extrapolate this scale to masses which most probably will be quite different from the original vector boson mass itself (*e.g.* by a factor of more than two for the top mass measurement). Obviously, decays of other known resonances, such as J/ψ and Υ, will provide additional constraints, which will minimise, if needed, the interpolation errors towards lower masses. In this extrapolation proc-

ess from the known vector boson masses to the mass to be measured with high precision, cross-checks between the various systems and disentangling individual contributions to the systematic uncertainty on the absolute scale will be of prime importance to keep it as small as possible.

Based on the above considerations, one can conclude that a precise understanding of the mass scale in ATLAS will require first and foremost an accurate knowledge of the measurement scale in each of the major detector elements, as described below in Section 12.2 for the Inner Detector (electrons and muons), in Section 12.3 for the EM Calorimeter (electrons and photons), in Section 12.4 for the Muon System, and in Section 12.5 for the overall Calorimeter (hadronic jets and $E_{\mathrm{T}}^{\mathrm{miss}}$).

This will not be sufficient, and the best accuracy on the overall mass scale will eventually be achieved by requiring the combination of the information from different detectors and by over-constraining the problem through numerous cross-checks:

- The electron energy measurements will rely mainly on the EM Calorimeter, but the knowledge of the absolute electron energy scale will probably be constrained in an optimal way by combining high-statistics precision measurements in the Inner Detector and the EM Calorimeter.
- The muon momentum measurements will rely on the combination of the measurements in the Muon System and in the Inner Detector on an event-by-event basis, and the knowledge of the absolute muon momentum scale will be constrained in an optimal way again by combining high-statistics precision measurements in both systems.
- The measurements of the energy of hadronic jets will rely on the overall ATLAS calorimetry over the range $|\eta| < 3.2$. In order to constrain to the required accuracy the jet energy scale over this region covered by several very different calorimeter technologies, it is expected that E/p measurements using isolated high-p_{T} charged hadrons from τ-decay will provide, in a first step, a quite powerful tool to transfer the scale, as known from the test-beam measurements, to the actual detector, to inter-calibrate the various calorimeter technologies, and possibly to constrain the absolute scale of the energy measurements for isolated charged pions (see Section 5.4). The transfer of this absolute scale to that of hadronic jets will require accurate and detailed Monte Carlo tools, as well as an excellent understanding of $W \rightarrow jj$ reconstruction in the hadronic calorimetry.

In the end, there can be only one mass scale for the whole ATLAS experiment and this will be determined by combining the various constraints from the individual systems and from the inter-calibrations between them.

One may expect that the Inner Detector momentum scale will be the most straightforward to calibrate, owing to the proximity of the measurement points to the primary vertex and to the magnetic nature of the measurement. However, systems which are situated further away from the primary vertex and with a rather large amount of material in front of them, such as the EM Calorimeter and the Muon System, will benefit from the very large statistics of $Z \rightarrow ee$ and $Z \rightarrow \mu\mu$ decays expected to be accumulated routinely (about 30 000 events per day at low luminosity) as a part of the inclusive triggers for many new physics searches. In addition, the even larger statistics of $W \rightarrow e\nu$ and $W \rightarrow \mu\nu$ decays, which will also be accumulated with high efficiency, will allow very precise cross-calibrations of these detectors with the Inner Detector.

The following sections present the results of the first attempts at establishing a strategy to achieve the above goals in the various systems composing the ATLAS detector and to combine the individual experimental measurements and scale uncertainties into an overall mass scale and its uncertainty.

12.2 Inner Detector scale

12.2.1 General considerations

As discussed above, the momentum scale in the Inner Detector (ID) should be known to an accuracy of 0.02% to obtain the desired precision on the measurement of the W mass. The implications of these requirements are examined in some detail for the Inner Detector in [12-3] and can be summarised as follows (this assumes that the absolute momentum scale is set using $Z \rightarrow ee$ and $Z \rightarrow \mu\mu$ decays for masses close to m_Z and that residual local effects average out to about 10% of their value over the whole detector):

- the ID alignment must be understood locally to ~1 μm on average in the bending plane;
- the solenoidal magnetic field must be understood locally to better than 0.1% on average;
- the amount of material in the ID must be understood globally to ~1% of its value (this is only required for $W \rightarrow e\nu$ decays);
- The ID p_T resolution must be understood globally to ~1%.

  This latter requirement has not been studied so far, but it seems rather straightforward to constrain the p_T resolution of the ID to the desired accuracy from the measured $Z \rightarrow \mu\mu$ mass distribution and from combined measurements of high-p_T electrons with the EM Calorimeter and of high-p_T muons with the Muon System.

The precise justification for the first three points is not easy to provide, since, as mentioned above and discussed in more detail in several of the following sections, the ultimate calibration of the overall scale will come from the use of the mass constraint in $Z \rightarrow \mu\mu$ decays. Systematics will, however, inevitably arise from not understanding details and hiding them in an all-encompassing calibration. It will therefore be essential to understand as well as possible all the individual components of the momentum determination; otherwise, small but not understood differences between *e.g.* the W and Z bosons will result in uncontrolled systematic uncertainties on m_W.

12.2.2 Alignment

The feasibility of meeting the above alignment requirement is very hard to demonstrate without real experimental data. Nevertheless, such an attempt has been considered in some detail in [12-3]; the main points are summarised below.

The use of reconstructed tracks and, in particular, of module overlaps in the Precision Tracker in the bending (R-ϕ) plane, to perform local alignment to an accuracy close to 1 μm, is described in detail in Section 3.7. Since the p_T of a track reconstructed in the ID alone is not known *a priori*, only certain distortions can be reconstructed through such procedures.

Even though the measurement points in the ID are quite uniformly distributed (in contrast to the Muon System, as discussed in Section 12.4), residual sagitta (or momentum scale) corrections will remain at some level. These cause shifts in the distributions of Q/p_T, where Q represents the charge of the reconstructed particle. Although the measured p_T spectra of oppositely charged particles could in principle be compared directly to correct for such shifts, this method is not precise enough in practice.

On the other hand, if the measured p_T spectra can be normalised by an estimate of p_T, then the uncertainties on the sagitta corrections can be greatly reduced. The estimate of p_T need not even be unbiassed: the only condition is that it should not be correlated to the charge of the particle. Given the very large statistics of high-p_T leptons expected to be accumulated by ATLAS, the EM Calorimeter measurements can be used to normalise p_T for electrons, and the Muon System measurements can be used to normalise p_T for muons, although charge-dependent biases will be more of a concern in this case than for the EM Calorimeter.

As discussed in [12-3], there will be enough statistics of $W \rightarrow e\nu$ decays and of LVL1 trigger muons of $p_T > 6$ GeV, to guarantee a statistical error for such measurements below the required accuracy of 0.02% after a few months of LHC operation at low luminosity. What remains to be demonstrated is that the systematic uncertainties associated to the correlation between the EM Calorimeter measurements and the electron charge, which are presumably quite small, and those associated to the correlation between the Muon System measurements and the muon charge, which are potentially much larger (see Section 12.4), can be controlled at the same level of 0.02%.

12.2.3 Magnetic field

Uncertainties arising from the imperfect knowledge of the scale of the magnetic field will feed directly into those on the absolute momentum scale (before calibration). To be confident that the calibration is well understood, it is desirable to reduce the uncertainty coming from the magnetic field to a level such that it does not mask other problems. A goal of better than 0.1% appears to be reasonable as a starting point.

The standard way to map a magnetic field such as that from the ATLAS solenoid is with a machine which scans an array of Hall and nuclear magnetic resonance (NMR) probes over the full ID volume. This will be done after all of the surrounding magnetic materials have been installed and just before the installation of the ID itself. The accuracy required is similar to that which has been achieved in the past (*e.g.* a measurement accuracy of 0.01% was achieved in [12-4] and an accuracy of the magnetic field map of a few parts in 10 000 was achieved in [12-5], although the desired goal was only 0.1%).

The ATLAS solenoid is more difficult to map than other solenoids because of its non-uniform field. NMR probes require uniform fields and hence will only function within ~70 cm from the centre. Therefore, over most of the ID volume, Hall probes will have to be relied upon. Hall probes can be calibrated to better than 0.05% (there is considerable on-going work within ATLAS to produce a large number of calibrated Hall probes to monitor the toroid field [12-6]). The high field gradients expected in the ID volume will require the position of the probes in the mapping machine to be known to ~0.5 mm, which is more precise than was necessary for previous maps. Some understanding of the field can be derived from simulation, but such calculations are typically only accurate to ~0.5%.

In addition to mapping the field at the time of installation, it will be essential to monitor it with the ID in place and during the lifetime of the experiment. The following effects may cause distortions of the field at the 0.1% level:

- Tiny quantities of ferro-magnetic material in the ID, which may be unavoidable, as for example nickel coating on the aluminium power cables, where they join the custom-made connectors on the SCT modules or at the level of the patch-panels.
- The mapping of the solenoid with the barrel toroid (most probably) switched off. Simulations predict that when the toroid is switched on, the solenoid field will decrease slightly because the extra field from the toroids will bring the Tile Calorimeter beams close to saturation and reduce their effectiveness at returning the solenoid field.

Other effects are considered to induce variations much smaller than 0.1%: para-magnetic and dia-magnetic effects due to the other components of the ID, the Earth's magnetic field, variations in the positions of the end-cap Calorimeters relative to the barrel Calorimeter when they are opened and shut, and hysteresis of the iron components.

The first-order effect of ferro-magnetic material (provided that it is uniformly distributed) and of the barrel toroid field, is to change the scale of the solenoid field map without changing its shape. This scale could be measured by building a small number of NMR probes into the SCT Barrel [12-7]. Such a system of probes would also provide a check of the position of the ID relative to the central axis of the magnetic field, which would be useful if the position of the solenoid coil were not absolutely stable.

Rather than simply measuring the field at a set of points in space, it would be preferable to describe it in terms of components satisfying Maxwell's Equations: $\nabla \cdot B = \nabla \times B = 0$. These components could be constrained using the combination of data from: the field map, the monitoring probes and pairs of reconstructed charged particle tracks from the decays of resonances of known mass (J/ψ, Y, Z). One set of functions, suitable for axial symmetry [12-4], are the modified Bessel functions, I_0 and I_1, expressed as a function of radius, R, and of position along the beam, z:

$$B_z = \sum_i a_i \cos\frac{iz}{c} \; I_0(\frac{iR}{c})$$

$$B_R = \sum_i a_i \sin\frac{iz}{c} \; I_1(\frac{iR}{c}).$$

In practice, the constraint of axial symmetry would probably need to be relaxed for the actual field configuration in the ATLAS ID. As an exercise to test the feasibility of fitting the field, an attempt was made to fit the simulated field. Despite using eight terms, the fit was poor and unstable, suggesting that more terms are needed. Better results were achieved starting from a field corresponding to an ideal solenoid. A scale factor was associated with this field, which was then augmented by two terms from the above power series.

The residuals between the fitted and simulated fields are shown in Figures 12-1 and 12-2, respectively for the axial and radial field components. The comparison is shown at a radius R = 75 cm, where the field deviates more strongly from uniformity than along the beam axis. It can be seen that, over most of the length of the coil, the field can be described to better than ±0.02%, corresponding to ±4 Gauss. There are significant deviations at values of $|z|$ larger than 2.6 m (the actual half-length of the solenoid coil is 2.65 m), but these would cause little effect on the momentum determination because they occur at the end of a track.

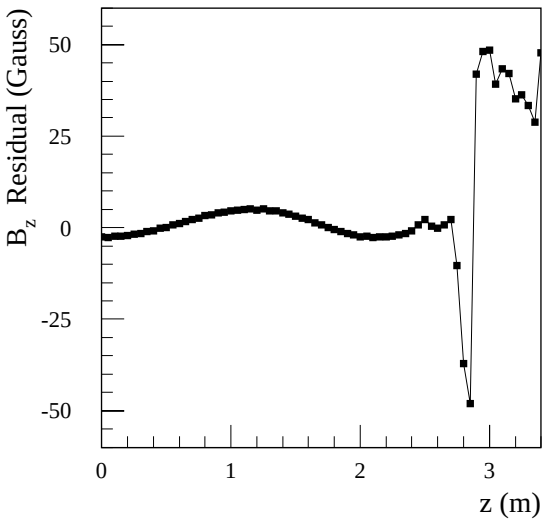

Figure 12-1 Difference between simulated and fitted axial magnetic field (B_z) components of the solenoid at a radius R = 75 cm.

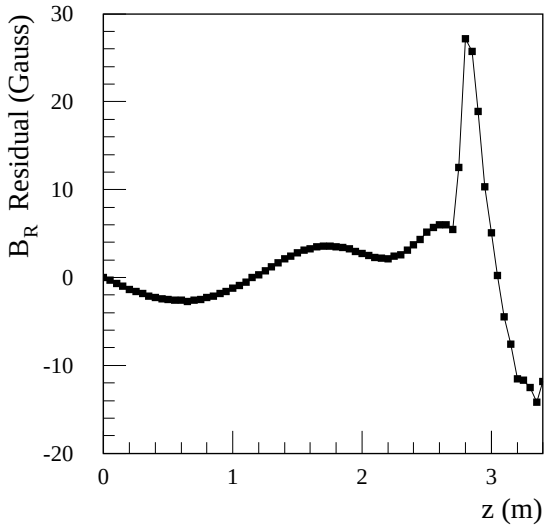

Figure 12-2 Difference between simulated and fitted radial magnetic field (B_R) components of the solenoid at a radius R = 75 cm.

12.2.4 Material in the Inner Detector

Material in the Inner Detector affects directly the momentum reconstruction for electrons, the energy reconstructed in the EM Calorimeter, and the *E/p* calibration, since the momentum as measured by the Inner Detector is subject to bremsstrahlung effects. Hence, the large amount of material present in the Inner Detector, if not known precisely enough (see also Section 12.3.1.1), might contribute significantly to systematic uncertainties on the knowledge of the absolute scale of the EM Calorimeter.

There are many approaches to determining the amount of material in the ID, all of which will be pursued:

- at the present stage of the detector construction (finalisation of detailed design), the amount of material in the ID is considered to be known to better than 5%, despite inevitable uncertainties in the most difficult areas (exact make-up of hybrids and chips, services and connectors, *etc.*);
- during construction, these estimates will be carefully updated by weighing detector components and assembled units. Valuable reference measurements will be provided in many cases by X-ray sources;
- *E/p* measurements with electrons from $W \rightarrow e\nu$ decay are described in Section 12.2.4.1;
- photon conversions are described in Section 12.2.4.2.

12.2.4.1 Use of *E/p* measurements with electrons from $W \rightarrow e\nu$ decays

The combined measurement of *E/p* with isolated high-p_T electrons from $W \rightarrow e\nu$ decays, using the EM Calorimeter and the Inner Detector, will be a key element to ensure a reliable comparison of the absolute momentum scale of the ID and of the absolute energy scale of the EM Calorimeter (see Section 7.2.2.2). This approach will complement the direct calibration of the absolute scale of the EM Calorimeter using $Z \rightarrow ee$ decays (see Sections 4.6 and 12.3).

The use of the shape of the electron *E/p* distribution to determine the amount of material in the Inner Detector is discussed in Section 7.2.2.3. The sensitivity of the peak of the *E/p* distribution, used for these calibrations, is such that, to understand the calibration of the EM Calorimeter to an accuracy of 0.02% will necessitate that the ID material must be understood to an accuracy of ~1% of its total value. This does not mean that every single item in the ID must be known this accurately, but the amount of material in regions of size of a few centimetres must be known to this precision. Like the EM Calorimeter energy measurements, the *E/p* calibration will be most sensitive to material at low radii, which is fortunately also the region where there will be the greatest sensitivity for determining in detail the material distribution.

It is shown in Section 7.2.2.3 that 10^6 reconstructed $W \rightarrow e\nu$ decays constitute a sufficient statistical sample to understand the ID material distribution to the required precision of ~1% of its total value. The available statistics will be about 30 times larger for one year of operation at low luminosity. In addition, high-purity samples of inclusive electrons (see Section 7.4), yet one order of magnitude larger in size than the $W \rightarrow e\nu$ sample, can also be used for such measurements (as shown for example in [12-1]), although only real data will demonstrate whether the required measurement quality and sample purities can indeed be achieved.

12.2.4.2 Use of photon conversions

The most obvious way to determine the amount of material in the Inner Detector is to look at the conversion rates (see Section 7.5.1). To obtain an absolute determination of the amount of material with this method requires a known rate of photons. Although this might be obtained from $Z \rightarrow ee\gamma$ decays, for which the topology is such as to give an easily identifiable photon, there will not be enough events of this type to obtain a map of the ID material to the desired accuracy.

An obvious alternative would be to use photon conversions from much more abundant sources, such as isolated high-p_T photons from direct photon production or even the very large statistics of lower-energy photons (mostly from π^0 decays), which are present in most events. Both these samples can be used for high-statistics relative measurements of the amount of material, as shown in Figures 12-3 and 12-4. Eventually, it is probable that an absolute measurement will be extracted from these samples, but it will require a reference object corresponding to a precisely known position and amount of material.

Figure 12-3 shows the radial positions of photon conversions of p_T = 50 GeV, as reconstructed in the barrel part of the ID. The three pixel barrel layers at their respective radii of 4, 11 and 14 cm, a support cylinder at a radius of 25 cm, and the first two SCT barrel layers at their respective radii of 30 and 38 cm can be clearly distinguished above the very small background. The beam pipe and the pixel *B*-layer are barely resolved. The cut-off in Figure 12-3 around the third SCT barrel layer is due to the requirement that a reconstructed track have at least four SCT hits.

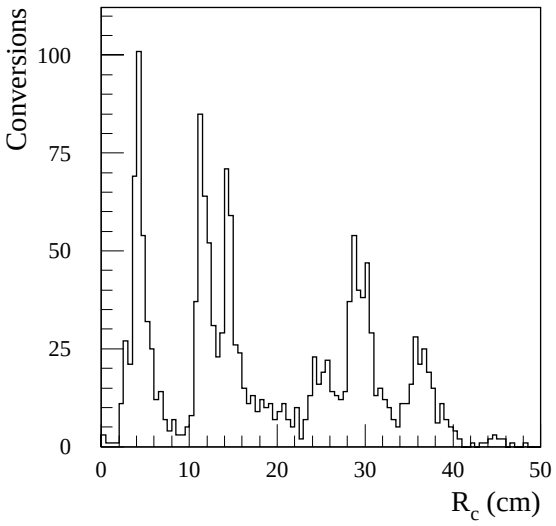

Figure 12-3 Reconstructed radial positions for conversions in the barrel part of the ID.

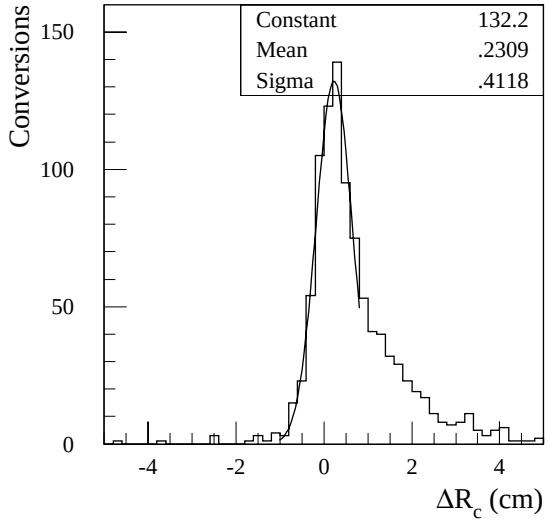

Figure 12-4 Difference between true and reconstructed radial position of conversions arising from p_T = 50 GeV photons which convert with R_c < 20 cm.

The width of the peaks in Figure 12-3 is dominated by the resolution on the radius of the reconstructed photon conversion, but is also affected by the effects of the azimuthal tilts of the planar detectors. Figure 12-4 shows the radial resolution for conversions in the pixel barrel layers. The resolution is ~4 mm, although there is a significant tail due to bremsstrahlung of the conversion electrons. In the first two barrel layers of the SCT, this resolution degrades somewhat to ~6 mm. Studies of photon conversions in *b*-jets, where the photon energies are much smaller, indicate that the radial resolution improves at lower p_T, as might be expected from the larger angular separation between the electrons. At very low p_T, the radial resolution is dominated by multiple scattering effects. Photon conversions can be reconstructed at larger radii, up to $R_c \approx 80$ cm, using the TRT alone (see Section 7.5.1), but the radial resolution is significantly degraded.

To determine the material at a given position, it is necessary to compare the number of reconstructed photon conversions at that position with the number reconstructed at the position of some reference object. This necessitates being able to resolve the position of the reference, which may not be trivial, as shown in Figure 12-3, because of the proximity of various layers and the modest radial resolution. Unfortunately, conversions in the beam pipe are not well resolved and may, when originating from π^0 decays, suffer from a significant Dalitz decay background. Although the statistics will be very large, a good understanding of the reconstruction efficiency of photon conversions will be essential, which will require in turn an improved conversion-finding program with higher efficiency.

12.2.5 Calibration with $Z \rightarrow \mu\mu$ and $Z \rightarrow ee$ decays

The general method described in Section 12.4.4 for the Muon System has not yet been applied to evaluate the accuracy with which the Inner Detector momentum scale could be constrained using $Z \rightarrow \mu\mu$ decays. In principle, residual sagitta corrections and the magnetic field components identified in Section 12.2.3 could be determined with this method by performing a global fit of the $Z \rightarrow \mu\mu$ sample, to which the constraint of the Z line-shape is applied. A similar but simpler

technique has been examined for the EM Calorimeter calibration with $Z \rightarrow ee$ decays (see Section 4.6). These techniques provide both an accurate inter-calibration between different parts of the detector, and an accurate estimate of the absolute mass scale at m_Z.

If one scales the statistical precision obtained using $Z \rightarrow ee$ decays over about 400 η–ϕ bins for the study of the EM Calorimeter calibration (see Section 4.6) to the expected statistics of 3×10^6 reconstructed $Z \rightarrow ee$ decays for one year of operation at low luminosity, this leads to a statistical precision of 0.02% in each of these η–ϕ bins. Since the experimental resolution for $Z \rightarrow \mu\mu$ decays reconstructed in the ID ($\sigma(p_T)/p_T \approx 2.1\%$) will be similar to that for $Z \rightarrow ee$ decays reconstructed in the EM Calorimeter ($\sigma(E)/E \approx 1.5\%$), it should be possible to understand the momentum scale in the ID with comparable statistical precision over a similar number of η–ϕ bins. It remains to be studied whether or not such a large number of bins would be needed for a measurement of the W mass to the required accuracy.

12.3 Electromagnetic Calorimeter scale

The EM Calorimeter scale is discussed here in terms of the uncertainty on the absolute energy scale of electrons and photons.

12.3.1 Determination of the electron energy scale with $Z \rightarrow ee$ decays

The use of $Z \rightarrow ee$ decays reconstructed solely in the EM Calorimeter, in particular to reduce the global constant term of the energy resolution, is described in detail in Section 4.6. From the results obtained in Section 4.6, it follows that about four years of data-taking at low luminosity would be needed to achieve an overall statistical accuracy of 0.02% per region of the EM Calorimeter with this method.

In this section, the basic sample of 50 000 fully simulated $Z \rightarrow ee$ decays described in Section 4.6 and a sample of 20 000 $Z \rightarrow ee$ decays, simulated with a modified layout of the Inner Detector, are analysed in terms of the uncertainties on the absolute energy scale of the EM Calorimeter. These uncertainties do not apply at the exact scale of m_Z, since this can be set to an almost arbitrarily good accuracy, but rather when attempting to transfer the absolute calibration at the Z mass to other masses. More specifically, both detector (material of the Inner Detector) and physics effects (inner photon bremsstrahlung, underlying event and pile-up) are examined below.

12.3.1.1 Material in the Inner Detector

The amount of material in front of the EM Calorimeter could affect directly the absolute electron energy scale, with the largest effects arising from external bremsstrahlung in the innermost layers of the Inner Detector. As discussed in Section 12.2.4, the description of the amount of material in the Inner Detector is estimated to be accurate to ~5% at the present stage of the detailed design of all components. This description will be refined during construction and will be carefully cross-checked *in situ*, using E/p measurements and photon conversions.

To evaluate directly the impact of an imperfect knowledge of the Inner Detector material on the calibration of the absolute energy scale of the EM Calorimeter, a sample of 20 000 $Z \rightarrow ee$ decays have been simulated, using a modified layout of the ID. This modified layout corresponds to an increase of the material in the support structures of the barrel and end-cap silicon microstrip detectors, ranging from ~15% in the barrel region to ~30% in the end-cap region. This increase is much larger than the 1% uncertainty, which could be obtained after a modest amount of data taking, using the methods discussed above.

The EM Calorimeter response has been compared to the nominal one, defined using the original sample of 50 000 $Z \rightarrow ee$ decays. As shown in Figure 12-5, the value of the reconstructed Z mass decreases by about 100 MeV.

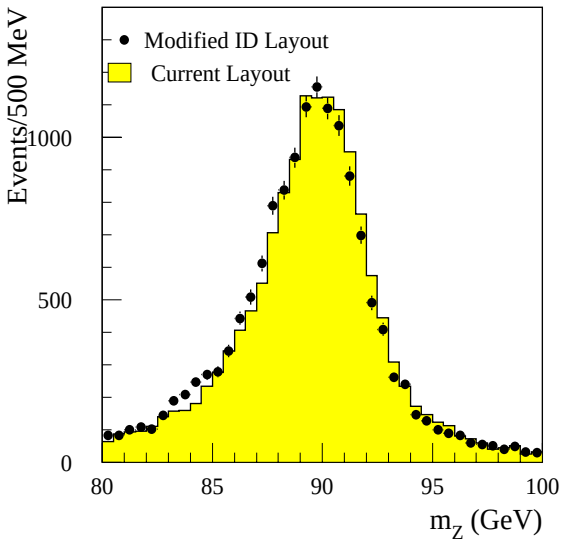

Figure 12-5 *Z*-boson lineshape, as reconstructed directly with the EM Calorimeter for the nominal Inner Detector layout (shaded histogram) and for a modified Inner Detector layout with ~ 20% more material in total (black dots).

As summarised in Table 12-1, if the results illustrated in Figure 12-5 were scaled to the estimated overall uncertainty of ~1% on the amount of material in the ID, the corresponding uncertainty on the electron scale should be around 5 MeV at the Z mass. This study has been performed by changing the amount of material in the silicon microstrip detectors. However, there is likely to be greater sensitivity to changes in the amount of material at even lower radii, namely in the pixel detectors. Table 12-1 therefore quotes a more conservative upper limit of 0.01% for the impact of the ID material on the determination of the absolute scale of the EM Calorimeter.

Table 12-1 Impact of Inner Detector material on the absolute energy scale of the EM Calorimeter.

Source of uncertainty	Uncertainty on electron energy scale at m_Z
Modified ID layout (material increased by 15-30%)	0.11%
Nominal ID layout (material known to 1%)	< 0.01%

12.3.1.2 Inner bremsstrahlung

The consequences of inner bremsstrahlung in $Z \rightarrow ee$ decays are:

- in a small fraction of events, the production of a high-p_T isolated photon in the final state will significantly distort the reconstructed mass spectrum of the two electrons. These events are easy to identify and to remove from the calibration sample;
- for a much larger fraction of events, the bremsstrahlung photon(s) remains very close to the electron shower, but slightly widens the transverse shower shape, thereby distorting slightly the reconstructed mass spectrum.

The reference sample of 50 000 fully simulated $Z \rightarrow ee$ decays has been generated using PYTHIA interfaced to PHOTOS [12-8], to account for photon emission through inner bremsstrahlung. To evaluate whether the distortions due to inner bremsstrahlung could be significant when compared to the calibration requirements, two additional $Z \rightarrow ee$ samples of 10 000 events each have been fully simulated, reconstructed and analysed, one without inner bremsstrahlung and one with forced photon emission (repeated calls to PHOTOS).

The reconstructed Z masses for these samples were then compared, after a cut on the shower width in the azimuthal plane was applied (see Table 12-2). By making a direct comparison to the sample of $Z \rightarrow ee$ decays, the reconstructed Z mass was found to be decreased by 70 MeV (or 0.08%) due to inner bremsstrahlung. The first-order calculations used at present for the inner bremsstrahlung are accurate to better than 10% (they could be greatly improved with more theoretical input), therefore the uncertainty on the absolute electron energy scale from this source is below 0.01%.

Table 12-2 Impact of inner bremsstrahlung on the absolute scale of the EM Calorimeter.

Sample of $Z \rightarrow ee$ decays and cuts used	**Relative shift of reconstructed Z mass**
Forced photon emission without cut on shower width	-0.33%
Forced photon emission with cut on shower width	–0.23%
Nominal photon emission with cut on shower width	–0.08%

12.3.1.3 Underlying event

Even though the size of the electromagnetic showers from $Z \rightarrow ee$ decays is quite small, a certain amount of energy from the underlying event is deposited in the calorimeter cells of interest in addition to that of the electrons themselves. The original sample of 20 000 $Z \rightarrow ee$ decays, which was generated with the default underlying event, was analysed a second time after a preprocessing stage, during which each event was superimposed onto itself after a 90° rotation in azimuth. Thus, the contribution of the underlying event to each 3×7 electron cluster in the EM Calorimeter was doubled. This procedure resulted in an increase of the reconstructed Z mass by 30 MeV or 0.03%. Since it will be possible to measure the properties of the underlying event with very large statistics, using the $Z \rightarrow ee$ events themselves, the contribution of this source to the uncertainty on the absolute energy scale for electrons can safely be neglected.

12.3.1.4 Pile–up

The EM Calorimeter readout uses a bipolar shaping and the response, averaged over the entire pulse duration is very close to zero, leading to very small average shifts of the measured energies due to pile-up (normalised to the average energy deposited per pile-up event). The exact values of these averages have been evaluated for every cell of the EM Calorimeter: they range from –1.7% to +2.1% at high luminosity, and from –3.1% to +3.6% at low luminosity (when optimal filtering is applied to reduce the electronic noise). The systematic shift of the absolute energy scale due to pile–up is therefore expected to be smaller than 50% (10%) of the effect of one

minimum–bias event at high (low) luminosity. Thanks to the bipolar shaping, these contributions are significantly smaller than the one from the underlying event, which has an activity typically a factor of two larger than that of a normal minimum-bias event.

12.3.1.5 Conclusions

The contributions of the most prominent sources of uncertainty on the EM Calorimeter scale for electrons are summarised in Table 12-3, which shows that the sum of all contributions can most likely be kept below 0.02%, which is the target set by the precision measurement of the W mass at the LHC (see Section 16.1). It should be noted once again that, at the scale of m_Z, none of the contributions in Table 12-3 matter much. However, they could contribute at some small level, as soon as the mass to be measured would be different from m_Z. In addition, other possible sources of systematic uncertainty, in particular those related to the multi-gain readout electronics of the EM Calorimeter, still remain to be studied and understood.

Table 12-3 Summary of the contributions to the uncertainty on the EM Calorimeter electron energy scale, as determined using $Z \rightarrow ee$ decays.

Source	Requirement	Uncertainty on scale
Material in Inner Detector	Known to 1%	< 0.01%
Inner bremsstrahlung	Known to 10%	< 0.01%
Underlying event	Calibrate and subtract	<< 0.03%
Pile–up at low luminosity	Calibrate and subtract	<< 0.01%
Pile–up at high luminosity	Calibrate and subtract	<< 0.01%

12.3.2 Determination of the photon energy scale using $Z \rightarrow ee\gamma$ decays

It is not clear from first principles that the absolute photon energy scale is identical to the electron energy scale to an accuracy of 0.1%. Additional constraints would be welcome, in particular if a Higgs boson decaying to photon pairs were to be discovered at the LHC. Possibly the only clean source of events which could be used to constrain the photon energy scale consists of $Z \rightarrow ee\gamma$ decays with a high-p_T photon well separated from the electrons. The use of the Z mass constraint could provide a sufficiently precise calibration tool albeit with somewhat marginal statistics.

This is illustrated in Figure 12-6, which shows the reconstructed spectrum of the invariant mass of the two electrons, m_{ee}, for the reference sample of 50 000 $Z \rightarrow ee$ decays, which includes the appropriate proportion of $Z \rightarrow ee\gamma$ decays. Also shown in Figure 12-6 is the distribution of m_{ee} for $Z \rightarrow ee\gamma$ decays with one photon with $p_T > 10$ GeV. It is important to note that more than 90% of the events with $m_{ee} < 70$ GeV are $Z \rightarrow ee\gamma$ decays: this indicates that the non-Gaussian tails from the reconstruction in the EM Calorimeter (events containing electrons in the barrel/end-cap transition region have been removed from the sample) and the low-energy tails from the Breit-Wigner line shape of the Z boson are both negligible with respect to the tails due to hard photons from inner bremsstrahlung.

For those events with $m_{ee} < 85$ GeV and containing a hard photon with $p_T > 10$ GeV, the measured energies of the photon and of the two electrons were rescaled in order to obtain $m_{ee\gamma} = m_Z$. As a result, the difference between the rescaled and measured photon energies has a resolution of ~0.8 GeV, averaged over all photons with $p_T > 10$ GeV.

The photons of interest in this section are typically those with $p_T \sim 50$ GeV from $H \rightarrow \gamma\gamma$ decay for $m_H = 100$ GeV. The p_T spectrum of inner bremsstrahlung photons in $Z \rightarrow ee\gamma$ decays decreases very rapidly as p_T increases, and only about 0.1% of $Z \rightarrow ee$ decays contain a reconstructed photon with $p_T > 30$ GeV. This would nevertheless lead to a total sample of 15 000 events for an integrated luminosity of 30 fb^{-1}, which would certainly provide the global statistics needed to be sensitive to a possible difference in scale at the level of ~10^{-3} between photons and electrons.

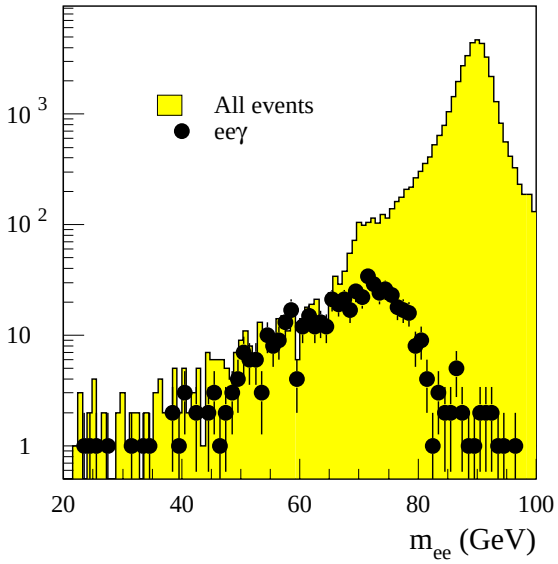

Figure 12-6 Distribution of the invariant mass of the two electrons from $Z \rightarrow ee$ decays reconstructed in the EM Calorimeter. The points with error bars denote events containing a hard photon with $p_T > 10$ GeV from inner bremsstrahlung. The statistics in the plot correspond to an integrated luminosity of 84 pb^{-1}.

12.4 Muon momentum scale

12.4.1 General considerations

The Muon System will provide high-precision and robust muon momentum measurements, which are almost completely uncorrelated with the Inner Detector measurements, since the magnetic bending occurs in different planes in the two systems. The various procedures involved in the determination of the absolute muon momentum scale and the level of precision that can be achieved are described below. Although the arguments in this section are developed specifically for the Muon System, the discussion on the calibration with $Z \rightarrow \mu\mu$ decays (see Section 12.4.4) applies also to a large extent to the calibration of the momentum scale of the Inner Detector (see also Section 12.2).

The momentum resolution and the absolute calibration of the Muon System measurements depend on the alignment of the precision chambers, the knowledge of the magnetic field, and the knowledge of the muon energy loss in the calorimeters. Since the track curvature measurement in the Muon System is obtained from only three points, the measurements themselves provide no redundancy, and an *in situ* check / recalibration of the Muon System with reconstructed tracks will require some knowledge of the incoming track curvature. This additional information can be provided by three methods:

- special runs without magnetic field (straight tracks to check and calibrate the alignment system), assuming they do not introduce additional uncertainties;
- a comparison with the momentum measured in the Inner Detector;

- the use of $Z \rightarrow \mu\mu$ decays, for which the precisely known Z mass provides strong constraints on the unknown parameters which may affect the measurements of the muon momenta.

Sections 12.4.2 and 12.4.3 respectively discuss the level of accuracy which can be achieved concerning the alignment of the precision chambers and the magnetic field, using special runs with straight tracks and the direct measurements provided by dedicated systems (Hall probes on the chambers and optical alignment system). Section 12.4.4 demonstrates how the calibration of the magnetic field and the energy loss in the calorimeters could be considerably improved by making use of $Z \rightarrow \mu\mu$ decays.

12.4.2 Alignment of the precision chambers

The alignment of the precision chambers is required to be sufficiently accurate, that the alignment contribution to the final measurement error (30 μm sagitta accuracy) remains well below the contribution from the intrinsic chamber measurement error (50 μm sagitta accuracy). The alignment system is based on optical straightness monitors (see [12-9] for an overview). The dominant uncertainty arises from the positioning of the optical sensors on the precision chambers or on carbon-fibre bars, the precision of which has to be better than 20 μm. In principle, the errors in the positioning of the sensors are supposed to be unbiased and randomly distributed over the chambers; therefore, it is hoped that the corresponding systematic error on the sagitta measurement, averaged over the complete system, could be below 2 μm, corresponding to a relative error of 0.02% on the sagitta at 50 GeV.

Alignment with reconstructed tracks will also provide strong constraints on possible residual systematic sagitta errors which would affect the absolute momentum scale. At the start of the experiment and after each major shutdown, it is planned to use straight muon tracks (data taken with the toroidal magnetic field off) to check the alignment systems and eventually to provide effective corrections which should account for errors in the positioning of the sensors on the chambers or on the bars. This may also correct for other spurious effects like local temperature gradients, provided that they are identical for field-off or field-on conditions.

The principle is to select muons with $p_T > 10$ GeV, with the toroids turned off and the solenoid field turned on (for track selection at LVL2 and beyond). In this way, the corrections to the sensor positions can be deduced from a comparison of the apparent track sagitta, as measured with the precision chambers, to the predictions of the optical alignment system. Given that the sensor positions on the chambers will be very stable, this correction map should be applicable to data taken with normal field conditions.

It should be stressed that the residual field from the magnetised iron has to be controlled to ~20% during the field off runs to reach the target resolution. Maintaining any systematic effect on the sagitta correction below 2 μm may require an even better control of these fields. Since the residual field from the iron girders does not extend significantly beyond a radius of 600 cm (in the barrel part of the system), a control of this residual field to 2 Gauss would be good enough to keep the relative effect on the sagitta below 0.02%.

Preliminary simulation studies have shown that this correction procedure can be implemented easily for the barrel part of the Muon System, where the alignment rays are almost purely projective. At low luminosity, enough statistics are collected in less than an hour to achieve a precision of 30 μm on the sagitta correction for sensors positioned up to 1 mm from their nominal position. For the Muon System end-caps, the larger departure from projectivity makes the correction less straightforward. Sagitta precisions around 30 μm seem to be a reasonable target, provided that the positioning of the sensors is better than 150 μm.

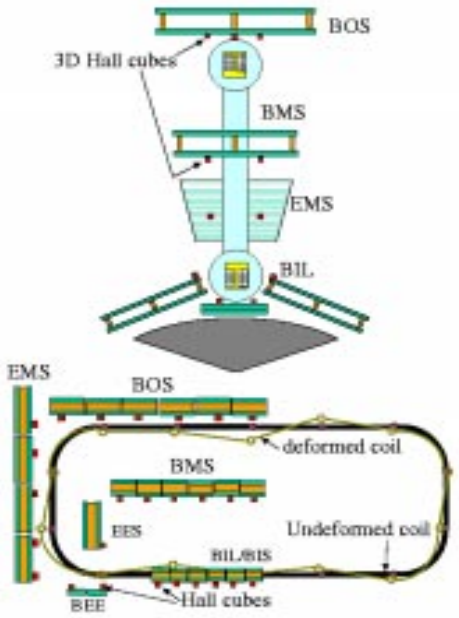

Figure 12-7 Sketch in two views of the layout of the mesh of 3D Hall probes mounted on the precision chambers (BEE, BIL/BIS, BMS, BOS, EES, EMS).

12.4.3 Magnetic field

In order to measure the field under running conditions, with all detector components in place and under the mutual influence of the different magnets and of magnetic materials (these are mainly the Tile Calorimeter and the iron girder serving as return yoke for the solenoid flux), the Muon System will be equipped with an array of Hall probes [12-9]. The proposed monitoring and measuring system consists of an arrangement of about 1500 sensors, accurately mounted on the precision chambers, where three orthogonal faces are equipped with a Hall probe to measure locally the three field components. The readings will be compared with 3D calculations and used for reconstructing the position and the shape of the toroid conductors with respect to the chambers (see Figure 12-7). The Hall probes are mounted directly on the precision chambers, so that they will at any moment provide the information on the actual position of the conductors with respect to the reference for the precision measurements, namely the precision chambers themselves.

Preliminary simulation studies using a simplified coil deformation model have shown that the magnetic field can be determined to a relative accuracy of 0.2% [12-9]. For these studies, the accuracy for positioning the probes was conservatively assumed to be 1 mm and 3 mrad. The accuracy of the absolute calibration of the probes was assumed to be 5 Gauss. This could be improved by at least a factor of two, if a temperature control at the level of 1 K is achieved.

Limitations coming from the coil deformation model and the imperfect treatment of the iron contribution to the magnetic field have to be investigated. A successful experimental test of the field reconstruction method based on the coil shape / position reconstruction has been done with a small (200x50 cm) prototype of a toroid coil, the so-called ‘race-track’ coil [12-10]. Further studies will be done in this direction with the B0 prototype coil.

The relative precision provided by direct measurements of the magnetic field will be limited most likely to about 0.1%.

12.4.4 Calibration with $Z \rightarrow \mu\mu$ decays

12.4.4.1 Introduction

As pointed out in Section 12.4.3, a precision better than 0.1% on the absolute muon momentum scale is probably out of reach for the direct magnetic field measurements. In addition, for measurements with the Muon System, the average energy loss in the calorimeters of ~4 GeV would have to be known with an accuracy of 10 MeV to reach the ultimate target of 0.02% for the *W* mass measurement. Although this may not be totally impossible, it would require dedicated measurements to improve the present knowledge and a very detailed description of the material in the calorimeters.

The only handle to improve the knowledge of the absolute muon momentum scale beyond the level of 0.1% is the abundant rate of $Z \rightarrow \mu\mu$ decays, which provides isolated muon pairs over a wide range of p_T and with a very small background contamination (*e.g.* from $Z \rightarrow \tau\tau$ decays).

The absolute calibration of the Muon System depends on the alignment of the precision chambers, the magnetic field measurements and the muon energy loss in the calorimeters. The muon momentum can be expressed in terms of various calibration parameters, which, for each tower of size ($\Delta\eta$, $\Delta\phi$), will control the alignment, the distortions of the magnetic field *B* and the average energy loss in the calorimeters.

For a muon *j* traversing the chamber tower *i*, the measured momentum, p_j^{meas}, can be expressed as:

$$p_j^{meas} = \frac{K_i \alpha_i B_i}{s_j + \delta x_i} + \lambda_i \varepsilon_i(p_j) \qquad 12\text{-}1$$

where α_ι is a field scale factor, s_j is the true sagitta, δx_i represents the tower misalignment, $\varepsilon_i(p_j)$ is the average energy loss as a function of momentum and λ_i is a scale factor for the average energy loss in tower *i*.

Equation 12-1 shows that, in principle, by using resonances decaying into muons with a wide momentum spread, the calibration permits the determination of all three effects (alignment, magnetic field and energy loss). In practice, given the limited statistics of the presently available fully simulated events, it will be assumed that the alignment is perfect and the calibration procedure will be restricted to the retrieval of the magnetic field and energy loss scale factors. In addition, Equation 12-1 includes only one unknown parameter per tower to describe the misalignment whereas, in general, six parameters are required.

From the conservation of 4-momentum, the following equations (p_1 and p_2 are the absolute values of the momenta of the two muons) can be obtained:

$$m_{12}^2 = m_Z^2 = 2 p_1 p_2 F(\theta_1, \phi_1, \theta_2, \phi_2)\,, \qquad 12\text{-}2$$

where ϕ_i and θ_i (i=1, 2) are the angles of the muon track at the vertex (these angles are determined by extrapolating the reconstructed muon track back from the muon system through the calorimeters and the Inner Detector to the vertex).

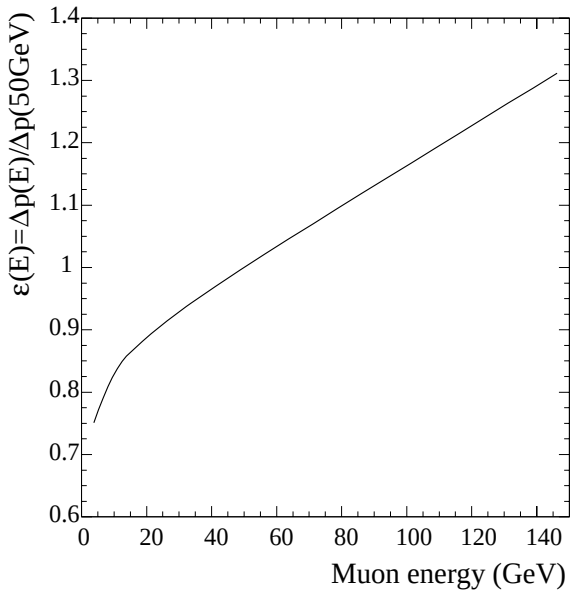

Figure 12-8 Mean energy loss, ε(*p*), of muons in iron as a function of the muon momentum *p*, normalised to the value ε(*p*) =1 at a momentum of 50 GeV.

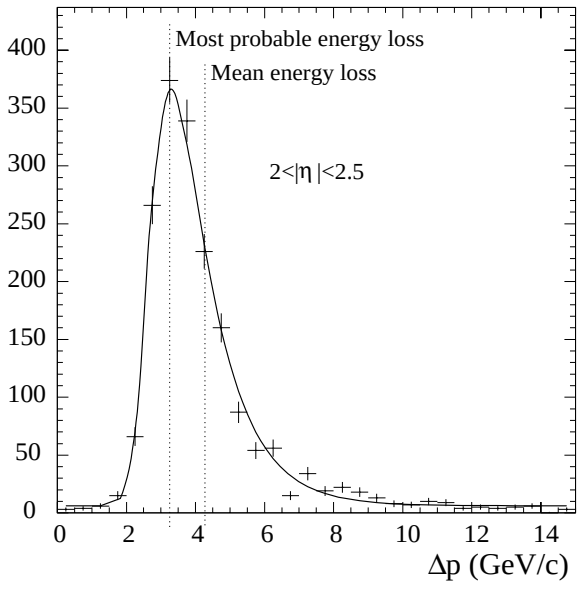

Figure 12-9 Generated energy-loss distribution in the calorimeter for 2 < |η| < 2.5.

12.4.4.2 Energy loss

The energy loss of muons in material is a function of the muon energy. This function was simulated for different materials in [12-11]. Figure 12-8 shows the normalised mean energy loss in iron, ε(*p*). Figure 12-9 shows the energy-loss distribution obtained from full simulation for muons in the range $2 < |\eta| < 2.5$, which agrees well with the distribution measured in an earlier hadronic calorimeter prototype [12-12]. In the calibration procedure presented here, only the mean energy loss is taken into account.

In the following, the energy loss of a muon is factorised into the momentum-dependent and the angle-dependent parts:

$$\Delta p(p, \theta) = \varepsilon(p) \cdot \Delta p(\theta)$$

where $\Delta p(\theta)$ is the average energy loss of a 50 GeV muon with polar angle θ. In this study, given the rather low statistics available, the small azimuthal dependence of the average energy loss has been neglected. The calibration algorithm described below would not have to be changed in any major way to introduce an azimuthal dependence of the energy loss.

12.4.4.3 Scale factors for the magnetic field

The roughly toroidal magnetic field in the Muon System will be measured by using about 5000 Hall probes, which will determine the field components locally (see Section 12.4.3). By performing a χ^2 minimisation, the position and shape of the coils can be retrieved. Using this information, supplemented by the calculated contributions from various surrounding magnetic materials, a nominal magnetic field map can be built.

This procedure provides a detailed description of the toroidal magnetic field. However, there is no way to exclude systematic errors due to unforeseen magnetic material or insufficient knowledge of its exact position. Such systematic errors may shift the absolute mass scale of the Muon System. Nevertheless, an effective correction can be done through the introduction of (η,ϕ) dependent scale factors. Since this study was limited to a large extent by statistics, only two scale factors are used, one for $-\pi < \phi < 0$ and one for $0 < \phi < \pi$.

12.4.4.4 Calibration algorithm and results

The algorithm which has been developed [12-13] allows the scale factors and the average energy loss to be obtained by minimising a likelihood function, which accounts for the finite width of the Z boson by the convolution of the Breit-Wigner with the resolution functions. Inner bremsstrahlung effects, which are significant, have not been taken into account in this first simplified approach.

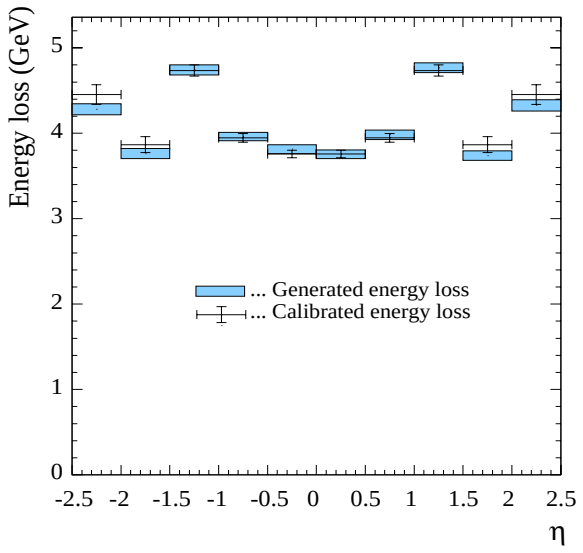

Figure 12-10 Generated and calibrated mean energy loss as a function of η for 50 GeV muons. The variations of the energy loss as a function of η reflect the varying amounts of absorber material in the calorimeters.

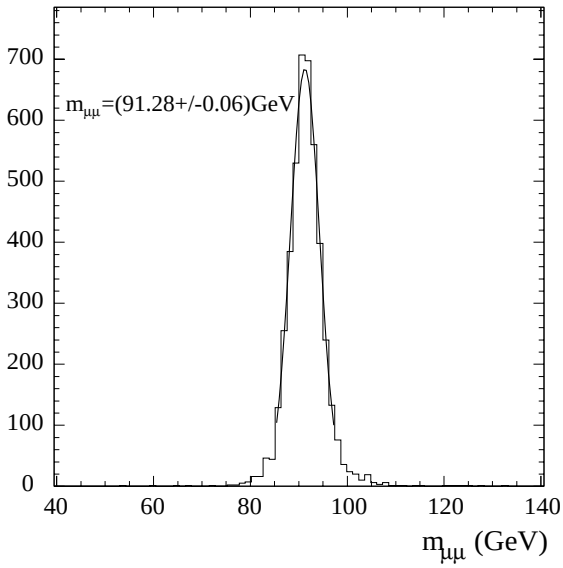

Figure 12-11 Reconstructed dimuon mass using the calibration results from Figure 12-10 and Table 12-4.

A sample of 10 000 $Z \rightarrow \mu\mu$ decays has been fully simulated and reconstructed. The magnetic field was changed by different scale factors α_i for different regions ($B \rightarrow B/\alpha_i$). Applying the method described above, it is possible to retrieve these scale factors with high accuracy and to calibrate the average energy loss as a function of pseudorapidity. The algorithm is reasonably independent of the chosen initial values. For this analysis, the initial values were generated by taking the generated values and smearing them by 10%.

A crucial point is the selection of good reconstructed tracks for the calibration. Since the energy loss obeys a Landau distribution, there are many events which have a huge energy loss and therefore a very small likelihood. Events with a likelihood below a certain cutoff were rejected, and the value of the cutoff was found empirically by minimising the number of iterations needed to converge.

For symmetry reasons, the mean energy loss was calculated as a function of pseudorapidity. The results of the likelihood minimisation procedure are displayed in Figure 12-10, which shows the mean energy loss for 50 GeV muons as a function of pseudorapidity. The calibrated energy loss is compared to the generated energy loss and shows excellent agreement. The accuracy is 45 MeV for small pseudorapidity (barrel region) and about 100 MeV for a pseudorapidity of 2. This accuracy will improve directly with the number of processed events.

Two magnetic field scale factors, $\alpha(\phi<0)$ and $\alpha(\phi>0)$, were fitted simultaneously and are retrieved with an accuracy of 0.1%, as shown in Table 12-4. To obtain the desired accuracy of 10 MeV for the average energy loss and 0.02% for the magnetic field scale factors, the number of events per (η,ϕ) channel (here $2\times5 = 10$ channels) has to be increased by approximately a factor of 40.

Table 12-4 Result of the calibration of the two magnetic field scale factors (the errors are statistical).

Sectors	$\phi < 0$	$\phi > 0$
Generated scale factors	1.01	0.98
Reconstructed scale factors	1.0103 ±0.0009	0.9816 ±0.0013

Figure 12-11 shows the Z mass reconstructed using the results of this calibration. The reconstructed mass is slightly too high, which is due to the fact that the mean energy loss was used (the most probable energy loss is smaller).

12.4.5 Conclusions

In this section, it has been shown that, even with very limited statistics (10 000 $Z \rightarrow \mu\mu$ decays) compared to that expected at the LHC, the absolute muon momentum scale can be calibrated to an accuracy of 0.1%. How the final errors scale with the available statistics will depend mainly on the number of (η,ϕ) channels for the magnetic field and energy loss scale factors. This motivates the efforts presently devoted to designing the best possible set of measurements and reconstruction of the magnetic field map in order to reduce the number of magnetic field scale factors.

If the determination of the absolute mass scale proves to be more accurate in the Inner Detector (see Section 12.2), the comparison of the momenta measured independently in the Inner Detector and in the Muon System may improve the calibration of the latter, or at the very least provide a very useful cross-check. The direct comparison is affected by the uncertainty on the average energy loss of the muons in the calorimeters. A comparison at the required level of 0.02% would need a knowledge of this average energy loss with an accuracy of 10 MeV (or 0.25% of the average loss) for a muon of 50 GeV energy. It will be extremely hard to achieve such an accuracy: dedicated energy-loss measurements with the various calorimeter materials would be necessary together with a very detailed knowledge of the materials composing the calorimeters.

A more promising procedure would make use of the difference between the momenta measured in both detectors, averaged over two separate samples of μ^+ and μ^-, selected to have identical distributions for their measured momentum in the Inner Detector. The quantity, $\langle p_{\mu S} - p_{ID}\rangle_+ + \langle p_{\mu S} - p_{ID}\rangle_-$, depends then only upon the average difference in energy loss between μ^+ and μ^-, which can be known to better than 10 MeV. If the Inner Detector is assumed to be perfectly calibrated, this quantity provides a direct estimate of the misalignment and / or of the magnetic field miscalibration in the Muon System.

12.5 Jet and E_T^{miss} scale

In this section, the absolute scale of the overall Calorimeter is discussed, mostly in terms of jet spectroscopy, but also for E_T^{miss} measurements relevant to reconstructed masses containing pairs of τ-leptons. As mentioned in Section 12.1, other Chapters deal with systematic effects possibly affecting the absolute energy scale of high-p_T jets at a scale of ~1 TeV.

12.5.1 Jet spectroscopy

12.5.1.1 General considerations

Many of the precision physics studies foreseen with ATLAS will involve decays of narrow resonances into hadronic jets, and the knowledge of the absolute jet energy scale will be one of the crucial ingredients determining the ultimate accuracy with which such measurements will be performed. This is a rather complex issue, because it is subject to both physics (initial- and final-state radiation, fragmentation, underlying event activity, jet algorithm, *etc.*) and detector (calorimeter response over a wide range of energies and over the full acceptance of the detector, non-linearities at high energies, *e/h* ratio, etc.) effects. All of these have to be understood at the level of a fraction of a percent in terms of systematic uncertainties, if the ATLAS goals for precision measurements in this sector are to be achieved.

As briefly summarised above in Section 12.1 and described in more detail in Chapters 5 and 9, a large fraction of the ATLAS calorimeter modules will have been calibrated in beams of electrons, muons and pions, before installation into ATLAS. *In situ* calibration using high-p_T isolated charged pions from τ-decays would guarantee an accurate and up-to-date inter-calibration between different modules and calorimeters (see Section 5.4). This will be needed over the pseudorapidity range $|\eta| < 3.2$, so the forward calorimeters are considered here only in connection with the knowledge of the absolute E_T^{miss} scale (see Section 12.5.2).

This wealth of calibration data will be one of the key elements in minimising the systematic uncertainties when reconstructing hadronic jets over a wide range of transverse energies and topologies. The next step in the understanding of the performance of the overall calorimetry in terms of jet spectroscopy will be to benefit from the unique features of the data samples which will be available at the LHC to perform an accurate *in situ* calibration of the absolute jet energy scale:

- For the case of light-quark jets, the very large statistics of $W \rightarrow jj$ decays from top quark decay will provide the best sample for understanding precisely the interplay between the jet energy scale and the mass scale of resonant jet-jet final states (the *W* mass will be known to an accuracy of ~30 MeV at the start-up of the LHC). It will also provide an almost perfect sample for constraining the top-quark mass when measured from purely hadronic final states (see Section 18.1.3).
- Events containing a *Z* boson decaying to leptons and one high-p_T jet will be very useful to cross-check the calibration of the jet energy scale performed with $W \rightarrow jj$ decays, and will also provide constraints on the *b*-jet energy scale, which cannot be obtained directly from top-quark decays. The use of γ+jet events had been considered in [12-14], since this sample could provide much higher statistics than the *Z*+jet sample, but the systematic uncertainties linked to residual background from hadronic jets misidentified as photons were

estimated to be too difficult to control at the required level and γ+jet events are not considered further here.

12.5.1.2 Use of $W \rightarrow jj$ decays

As stated above, the reconstruction of $W \rightarrow jj$ decays is the most promising tool for *in situ* calibration of hadron calorimetry at the LHC. The large $t\bar{t}$ cross-section will provide an abundant sample of hadronically decaying W bosons. For example, about 80 000 $t\bar{t}$ events will be produced per day at low luminosity, out of which approximately 1500 $l\nu jjb\bar{b}$ final states can be reconstructed (see Chapter 18). This sample can be cleanly separated from the dominant QCD W+jet and the electroweak WW backgrounds by requiring an isolated lepton with $p_T > 20$ GeV and at least four jets with $p_T > 40$ GeV, two of which are tagged as b-jets.

A sample of 45 000 events would be collected for an integrated luminosity of 10 fb^{-1}. The invariant mass of jets not tagged as b-jets is used to reconstruct the $W \rightarrow jj$ decay, as shown in Section 18.1.2 (the combination with the mass closest to the W mass is selected). After these simple kinematic cuts, the background under the peak is small and arises mainly from wrong jet-jet combinations in the signal events themselves. The optimal method to reconstruct the jet-jet mass for $W \rightarrow jj$ decays depends quite strongly on the transverse momentum of the W boson and on the physics goals. Several methods and their associated systematics are discussed in some detail in Section 9.3.1 (see also [12-15] for a detailed study). The discussion here limits itself to estimating with fast simulation the size of the systematic uncertainties affecting the absolute jet energy scale, before and after calibrating a high-statistics sample of $W \rightarrow jj$ decays to the known value of m_W.

For inclusive $t\bar{t}$ events with a reconstructed $W \rightarrow jj$ decay, Figure 12-12 shows, for each reconstructed jet from the $W \rightarrow jj$ decay, the ratio of the p_T of the original parton, p_T^{parton}, to the p_T of the reconstructed jet, p_T^{jet}, as a function of p_T^{jet}. The jets are reconstructed using a standard fixed-cone jet algorithm with a cone size $\Delta R = 0.4$ (optimised for high-luminosity operation) and the reconstructed jet-jet mass is required to be within ±15 GeV of the nominal W mass. Figure 12-12 shows the results obtained both with and without including QCD final-state radiation (FSR). Initial-state radiation and underlying event effects are very small. On the other hand, the effect of FSR is quite large for $p_T^{\text{jet}} \sim 50$ GeV because out-of-cone losses remain significant, *i.e.* of the order of 10% for these values of p_T^{jet}. For values of p_T^{jet} close to 200 GeV, the ratio $p_T^{\text{parton}} / p_T^{\text{jet}}$ tends to be smaller than unity. This effect is almost entirely recovered by requiring the opening angle between the two jets to be $\Delta R > 0.8$, indicating that effects related to overlap between the two jets become significant for $p_T^{\text{jet}} > 200$ GeV. This corresponds roughly to $p_T^W > 400$ GeV, for which it is well known from heavy Higgs boson searches that the jets from $W \rightarrow jj$ decay overlap significantly and therefore require a dedicated algorithm for the reconstruction (see Section 19.2.10).

The 4-vectors of the reconstructed jets from $W \rightarrow jj$ decay are then rescaled so that $m_{jj} = m_W$. The result of this procedure is shown in Figure 12-13. For values of $p_T^{\text{jet}} > 70$ GeV, this rescaling procedure to the known W mass achieves reasonably well the desired goal of a ±1% overall systematic uncertainty on the absolute jet energy scale. However, for $p_T^{\text{jet}} \sim 50$ GeV, residual systematic effects from FSR remain at the level of ~3%. These effects could be further reduced by using a larger cone, *e.g.* of size $\Delta R = 0.7$ at low luminosity, and / or applying a more refined rescaling procedure.

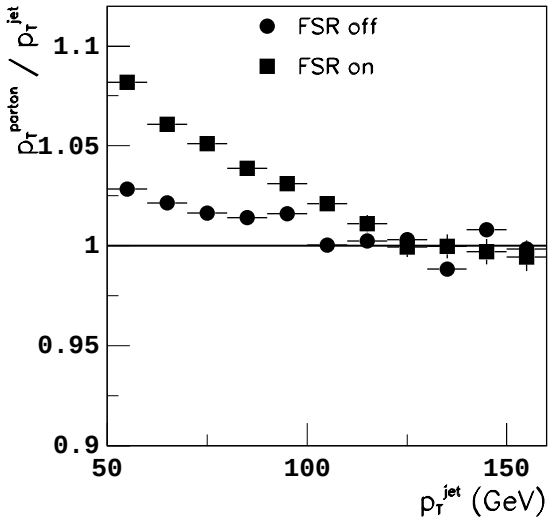

Figure 12-12 Ratio of the original parton p_T, p_T^{parton}, to the p_T of the reconstructed jet, p_T^{jet}, as a function of p_T^{jet}, for $W \rightarrow jj$ decays reconstructed in inclusive $t\bar{t}$ events. The black squares correspond to both initial-state and final-state radiation turned on, whereas the black circles are obtained in the case where final-state radiation (FSR) is switched off.

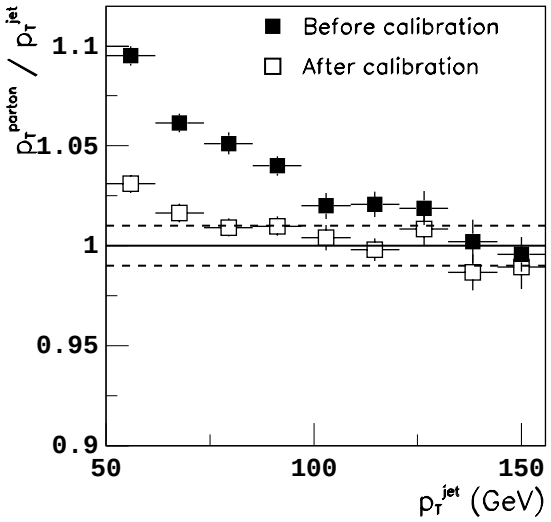

Figure 12-13 Ratio of the original parton p_T, p_T^{parton}, to the p_T of the reconstructed jet, p_T^{jet}, as a function of p_T^{jet}, for $W \rightarrow jj$ decays reconstructed in inclusive $t\bar{t}$ events. The black squares correspond to the case without rescaling, whereas the open squares correspond to the result after rescaling the jet 4-vectors to obtain $m_{jj} = m_W$ (see text). The dashed horizontal lines represent the desired goal of a ±1% systematic uncertainty on the absolute jet energy scale.

In conclusion, the high-statistics $W \rightarrow jj$ decays reconstructed in inclusive $t\bar{t}$ events should provide an adequate tool to achieve an overall ±1% uncertainty on the absolute jet energy scale, over a range of jet transverse momenta from 50 GeV to several hundred GeV. The lower and upper ends of this range will depend on how well residual systematic effects can be controlled with the data and the Monte Carlo simulation:

- for $p_T^{jet} \sim 50$ GeV, residual effects due to the interplay between final-state radiation and the fraction of the jet energy not collected by the specific algorithm used could be significant with respect to the desired goal;
- for $p_T^{jet} > 200$ GeV, residual effects due to overlap between the two jets from the W decay may also be significant. In addition, the constraints from the data will always be limited by statistics if one attempts to use only well-separated reconstructed jets in this case.

12.5.1.3 Use of *Z*+jet events

It has been shown at the Tevatron [12-16], that Z+jet events, containing $Z \rightarrow ee$ or $Z \rightarrow \mu\mu$ decays and one high-p_T jet, constitute a useful sample to constrain *in situ* the calibration of the absolute jet energy scale. The method is apparently quite simple and takes advantage of the expected balance in p_T between the precisely measured leptonic Z decay and the highest-p_T jet in the event.

Although the expected rates for this process at the LHC are quite large (see also Section 15.7.4), a clean selection of such events is not straightforward, because initial-state radiation often produces additional high-p_T jets, which degrades the quality of the p_T-balance between the Z boson and the leading jet. This is a source of potentially significant systematic uncertainties in the low-p_T region, where the probability for producing additional jets of comparable p_T is high.

A first step in the study of these Z+jet events is to define selection cuts, which preferentially select topologies with one and only one back-to-back jet produced in association with the Z boson. The impact of these cuts has been assessed using fast simulation by studying the evolution of the average fractional imbalance between the p_T of the Z boson and the p_T of the leading reconstructed jet, $(p_T^Z - p_T)/p_T^Z$, as a function of the cuts applied to the sample. These cuts are the following:

- the difference in azimuth, $\Delta\phi$, between the reconstructed Z boson and the leading jet is required to be $\Delta\phi > 3.06$;
- a loose jet veto requires that no additional jet with $p_T > 40$ GeV and $|\eta| < 3.2$ be reconstructed in the event (this jet veto can also be used at high luminosity), as shown in Section 9.1.3;
- a tight jet veto requires that no additional jet with $p_T > 15$ GeV and $|\eta| < 4.9$ be reconstructed in the event.

Table 12-5 Evolution of the average fractional imbalance between the p_T of the Z boson and the p_T of the leading jet in Z+jet events as a function of the selection cuts applied and of the successive ingredients used in the event generation. The results are shown for jets in the p_T range between 20 and 60 GeV (top line of each cell) and between 60 and 120 GeV (bottom line of each cell). The jets are reconstructed in a cone of size $\Delta R = 0.7$ (the last column shows the effect of increasing the cone size to $\Delta R = 1.0$).

Selection cuts	Hard process	+ underlying event	+ initial-state radiation	+ final-state radiation ($\Delta R = 0.7$)	+ final-state radiation ($\Delta R = 1.0$)
One jet with $p_T > 20$ GeV and $\|\eta\| < 3.2$	0.026 0.015	0.005 0.002	0.050 0.034	0.097 0.071	0.043 0.030
$\Delta\phi > 3.06$	0.026 0.015	0.005 0.002	0.023 0.014	0.050 0.042	0.020 0.007
$\Delta\phi > 3.06$ and loose jet veto	0.026 0.015	0.005 0.002	0.022 0.013	0.049 0.041	0.019 0.006
$\Delta\phi > 3.06$ and tight jet veto	0.026 0.015	0.005 0.002	0.018 0.011	0.044 0.033	0.014 0.002

The evolution of the average value of the fractional imbalance as a function of the cuts and of the successive ingredients used in the event generation (hard-scattering process, underlying event, initial-state and final-state radiation) is shown in Table 12-5 for Z+jet events with a leading jet with $p_T > 20$ GeV reconstructed in a cone of size $\Delta R = 0.7$. The following observations can be made:

- if no dedicated selection cuts are applied and all ingredients in the event generation are switched on, the average value of the fractional imbalance is about 10% for low-p_T jets in the range from 20 to 60 GeV, and decreases to about 7% for higher-p_T jets in the range from 60 to 120 GeV;

- the cut on $\Delta\phi$ improves the situation considerably, and a further significant but smaller improvement is obtained by applying in addition the tight jet-veto cut. The loose jet-veto cut does not improve the situation much, indicating that the Z+jet calibration method will be more difficult to benefit from at high luminosity;
- the impact of final-state radiation is the largest for the default cone size of $\Delta R = 0.7$, but the impact of initial-state radiation cannot be neglected even after all selection cuts. If a cone size of $\Delta R = 1.0$ were to be used, Table 12-5 shows that the expected average value of the fractional imbalance can be brought down to a level close to or below the desired goal of ±1%, even for low-p_T jets.

The distribution of the fractional imbalance is shown in Figures 12-14 and 12-15 for jets reconstructed with $60 < p_T < 120$ GeV, respectively before cuts and after applying the $\Delta\phi$ and tight jet-veto cuts described above. These figures show that the selection cuts not only decrease the average value of the fractional imbalance, but also improve considerably its spread.

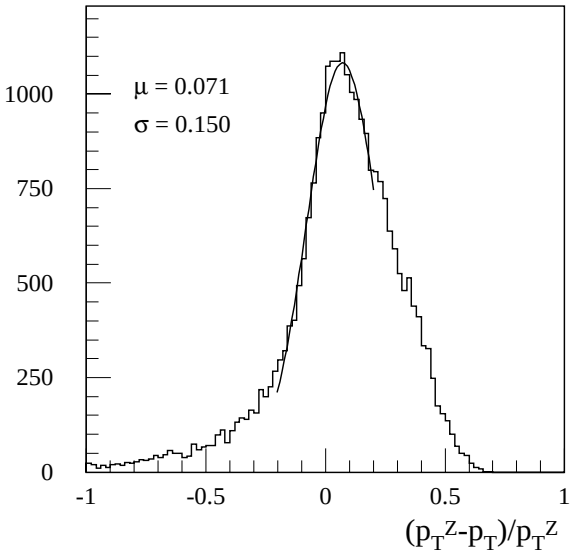

Figure 12-14 Fractional imbalance between the p_T of the Z boson, p_T^Z, and the p_T of the leading jet for Z+jet events with a reconstructed jet in the p_T range from 60 to 120 GeV before any further cuts are applied. A cone of size $\Delta R = 0.7$ is used to collect the jet energy.

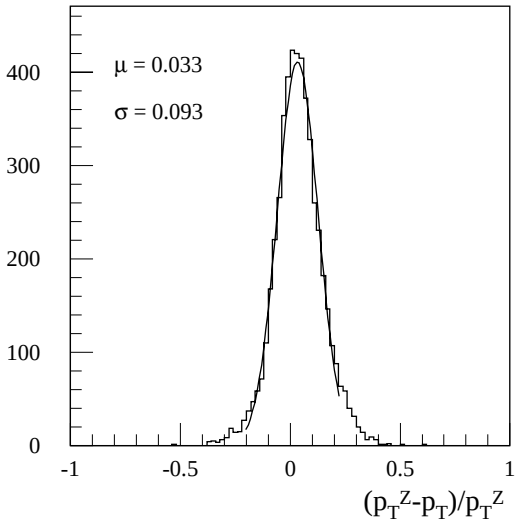

Figure 12-15 Same as Figure 12-14, but after the $\Delta\phi$ and tight jet-veto cuts listed in Table 12-5 have been applied.

The expected rates of Z+jet events passing the $\Delta\phi$ and tight jet-veto cuts of Table 12-5 are shown in Table 12-6 for an integrated luminosity of 10 fb^{-1} and for the various regions of the Calorimeter. These rates are fully adequate to obtain a statistical sensitivity at the required level of ±1% for jets of $p_T < 200$ GeV over the complete coverage, including even the Forward Calorimeter. More integrated luminosity would be needed to measure the response at the same ±1% level of accuracy for jets with $p_T > 200$ GeV. It should be noted that, for obvious reasons linked to the lower expected signal rates and to the lack of precise theoretical predictions, the precision on the absolute mass scale required by physics is not as tight at the scale of 500 GeV to 1 TeV as at the 50-100 GeV scale. Table 12-6 also shows the rates expected for Z+b-jet events, for which the b-jets are assumed to be tagged with an efficiency of 50% (see Chapter 10). The overall Z+jet sample contains a mixture of jet flavours with typically about 28% of gluon jets, 54% of light-

quark jets, 12% of *c*-jets and 6% of *b*-jets. With the *b*-tagging rejections reported in Chapter 10, the *Z*+*b*-jet samples of Table 12-6 should have a purity close to 90%, hopefully sufficient to constrain independently the absolute energy scale of *b*-jets to the same accuracy of ±1%.

Table 12-6 For an integrated luminosity of 10 fb^{-1}, expected rates for *Z*+jet (top line of each cell) and Z+*b*-jet (bottom line of each cell) events passing the $\Delta\phi$ and tight jet-veto cuts of Table 12-5, for three ranges of jet p_T and for the various regions of the ATLAS hadronic calorimetry. The rates for *Z*+b-jet events assume a *b*-tagging efficiency of 50%.

Region of calorimeter	$20 < p_T < 60$ GeV	$60 < p_T < 120$ GeV	$p_T > 120$ GeV
Barrel ($\|\eta\| < 1.0$)	190 000 5000	100 000 2000	24 000 500
Extended barrel ($0.8 < \|\eta\| < 1.7$)	150 000 3500	80 000 1500	20 000 500
End-cap ($1.5 < \|\eta\| < 3.2$) End-cap ($1.5 < \|\eta\| < 2.5$)	190 000 4500	90 000 1500	16 000 500
Forward ($3.2 < \|\eta\| < 4.9$)	30 000	10 000	1000

The use of the *Z*+jet events for an accurate determination of the jet energy scale seems therefore promising, based on the studies with fast simulation reported above. These studies have been complemented by (and cross-checked with) full simulation and reconstruction in the following way [12-17]:

- A sample of *Z*+jet events with $p_T^Z > 40$ GeV was fully simulated and reconstructed in the Calorimeters. This required a careful inter-calibration between the different regions of the calorimetry. Although this sample spanned the pseudorapidity coverage of the Calorimeters over $|\eta| < 3.2$, most of the statistics described here was concentrated in the barrel and extended-barrel regions.
- a very similar but much higher-statistics sample was simulated with fast simulation, essentially reproducing the results of Table 12-5 over a different p_T range.

These samples were then compared in terms of the fractional imbalance between p_T^Z and the jet p_T, as shown in Table 12-7. The agreement between the fast simulation and the full simulation / reconstruction is reasonable, although the jet veto cuts appear to reduce the fractional imbalance more strongly in the fully simulated events. This effect might be due to the difficulty of setting the energy scale accurately for low-p_T jets in the reconstruction.

Figures 12-16 and 12-17 show the distributions of the fractional imbalance before cuts and after the $\Delta\phi$ and tight jet-veto cuts listed in Table 12-7, respectively for the cases of fast and full simulation. These Figures show that the shapes of the distributions are also in good agreement between the fast simulation and the full simulation / reconstruction. Finally, Figure 12-18 shows the variation of the average fractional imbalance as a function of the jet p_T. The results display the progressive decrease of the residual imbalance due to initial-state and final-state radiation as the jet p_T increases.

The next step in assessing the usefulness of the *Z*+jet events for an accurate calibration of the absolute jet energy scale is to compare the reconstructed jet p_T, rescaled to balance the p_T of the *Z* boson, to the original parton p_T. Table 12-8 shows the fractional imbalance, calculated now from the reconstructed jet p_T, rescaled to balance the p_T of the *Z* boson, and from the original parton p_T, as a function of the successive selection cuts and for three ranges of jet p_T. Even after

Table 12-7 Evolution of the average fractional imbalance between the p_T of the Z boson and the p_T of the leading jet in Z+jet events as a function of the selection cuts applied. The results are shown for fast simulation (as in Table 12-5) and for full simulation and reconstruction, both for all jets and for b-jets. The statistical error on the numbers for the fully simulated sample is 0.01, whereas it is negligible for the fast simulation.

	Fast simulation (all jets)	**Full simulation (all jets)**	**Fast simulation (b-jets)**	**Full simulation (b-jets)**
One jet with $p_T > 40$ GeV and $\|\eta\| < 3.2$	0.053	0.057	0.106	0.089
$\Delta\phi > 2.99$	0.040	0.037	0.091	
$\Delta\phi > 2.99$ and loose jet veto	0.039	0.027	0.089	
$\Delta\phi > 2.99$ and tight jet veto	0.033	0.024	0.076	0.050

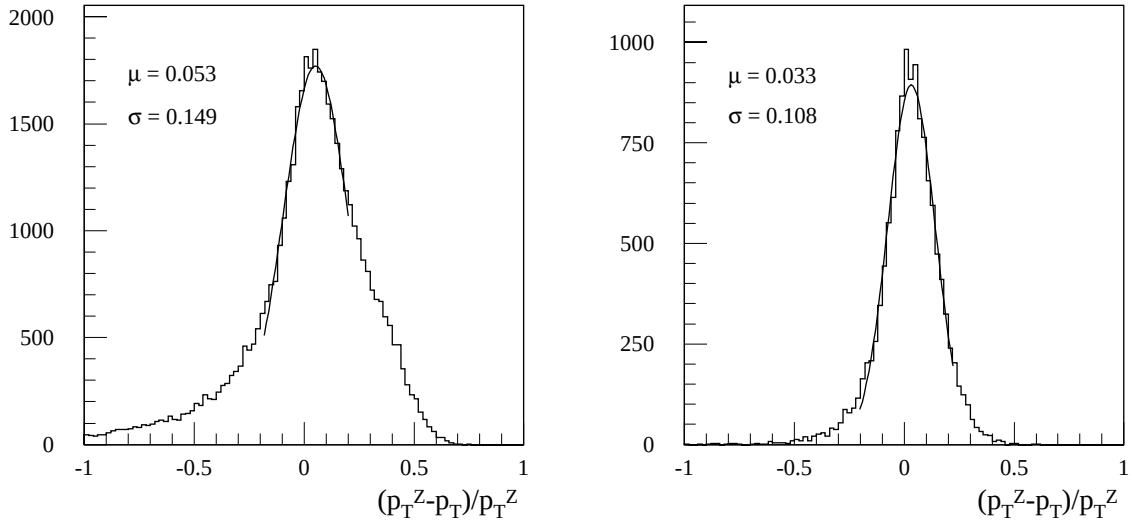

Figure 12-16 After fast simulation, fractional imbalance between the p_T of the Z boson, p_T^Z, and the p_T of the leading jet for Z+jet events containing a reconstructed jet with $p_T > 40$ GeV within $|\eta| < 3.2$, before (left) and after (right) the $\Delta\phi$ and tight jet-veto cuts listed in Table 12-7 are applied. A cone of size $\Delta R = 0.7$ is used to collect the jet energy.

all the selection cuts are applied, the residual fractional imbalance remains significant for jets with $p_T < 60$ GeV. The results shown in Table 12-8 show that the desired goal of an overall systematic uncertainty below ±1% on the absolute jet energy scale may be achieved only for jets with $p_T > 50$ GeV using Z+jet events.

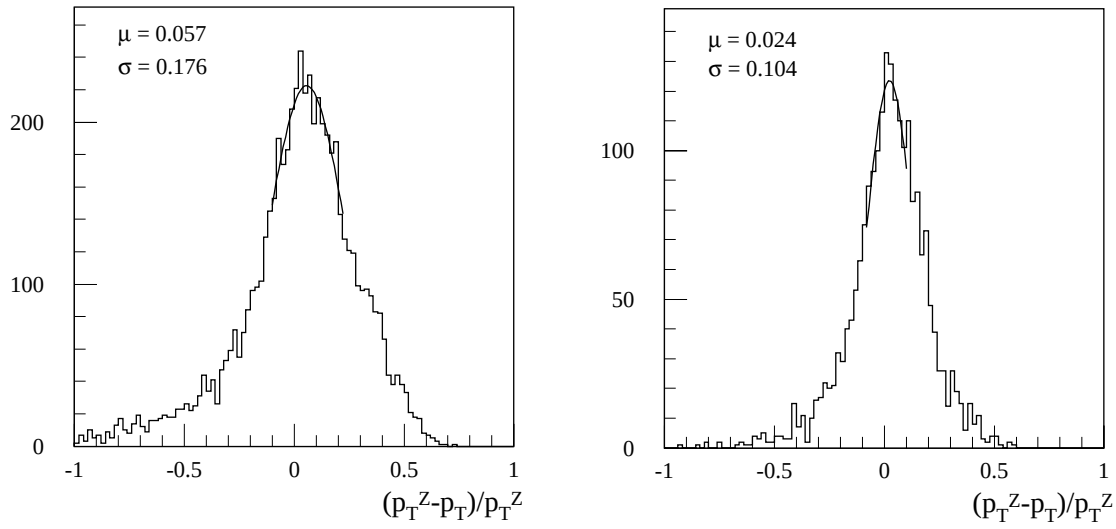

Figure 12-17 Same as Figure 12-16, but for full simulation and reconstruction.

Table 12-8 Evolution of the average fractional imbalance between the p_T of the leading jet in Z+jet events, rescaled to match the p_T of the Z boson, and the original parton p_T, as a function of the selection cuts applied and of the p_T range of the jets.

Jet p_T range (GeV)	20 < p_T < 60 GeV	60 < p_T < 120 GeV	p_T > 120 GeV
No cuts	0.163	0.060	0.011
$\Delta\phi > 3.06$	0.074	0.030	0.005
$\Delta\phi > 3.06$ and loose jet veto	0.071	0.026	0.004
$\Delta\phi > 3.06$ and tight jet veto	0.049	0.015	0.004

As a final step in the present study, the impact of the main sources of systematic uncertainties on the quality of the calibration with Z+jet events was studied. The possible systematic uncertainties arising from the detector response itself are described in Chapter 9 and are not considered here. Other sources of systematic uncertainties which may affect the calibrations using Z+jet events are:

- Uncertainties due to the modelling of initial-state radiation are probably dominant in this particular case. They have been estimated by varying Λ_{QCD} in the event generation by a factor 1.5 in either direction and the resulting variations on the average fractional imbalance, for Z+jet events passing the $\Delta\phi$ and tight jet-veto cuts, are between ±1.5% at low p_T and 0.3% at high p_T.
- Uncertainties arising from the imperfect modelling of the Z+jet events for back-to-back topologies have been estimated by tightening even further the $\Delta\phi$ cut from $\Delta\phi > 3.06$ to $\Delta\phi > 3.12$. The effect, in this case, is between -0.7% and -0.1%.

In conclusion, Z+jet events will be a useful high-statistics tool to cross-check the setting of the absolute jet energy scale using $W \rightarrow jj$ decays in $t\bar{t}$ events over a wide range of jet p_T. These events could also be used to set the absolute scale in the forward calorimeter, for which the standard method using $W \rightarrow jj$ decays does not apply. More studies are needed to ascertain better the limitations of the method and possibly to improve it by using the well-known technique of projecting the jet p_T onto privileged axes corresponding to the bisectors of the angle between the transverse momenta of the jet and of the Z boson. In addition, Z+jet events may provide a useful source for calibrating independently the b-jet energy scale, since high-statistics and 90% pure samples of Z+b-jet events should be obtained for an integrated luminosity of 10 fb^{-1}. Finally, Z+jet events may well also be of great importance to check the linearity of the overall Calorimeter as the jet p_T reaches large values in the TeV range.

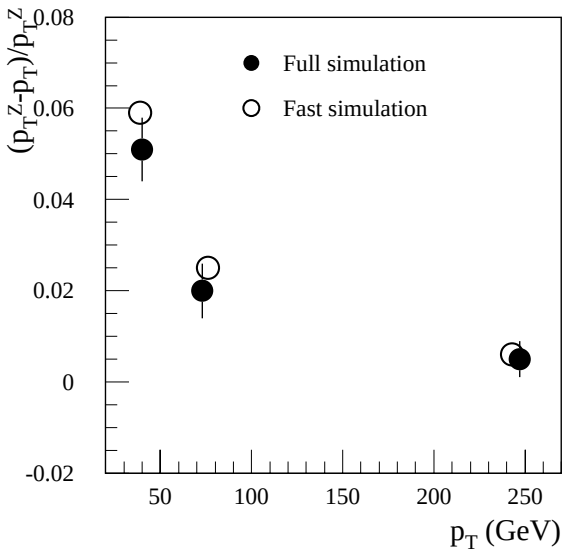

Figure 12-18 Average fractional imbalance between the p_T of the Z boson, p_T^Z, and the p_T of the leading jet as a function of the jet p_T. The results of fast simulation (open circles) and full simulation and reconstruction (black circles) are shown for Z+jet events containing a reconstructed jet with p_T > 40 GeV within $|\eta|$ < 3.2 and passing the $\Delta\phi$ and tight jet-veto cuts listed in Table 12-7. A cone of size ΔR = 0.7 is used to collect the jet energy.

12.5.2 E_T^{miss} and forward calorimeter scale

Once the absolute energy scale of the ATLAS Hadronic Calorimeter has been set to ±1% over the range $|\eta|$ < 3.2, following the methods described in Section 12.5.1, the knowledge of the absolute energy scale over the full pseudorapidity coverage, *i.e.* including the forward calorimeters, is mainly of interest for physics involving an accurate measurement of E_T^{miss} (the quality of forward jet tagging, *e.g.* as used in heavy Higgs-boson searches described in Section 19.2.10, depends mostly on an accurate measurement of the jet polar angle). The most prominent examples of such cases are the search for resonances decaying into pairs of τ-leptons (see Section 19.3.2.5) and to a lesser extent precision SUSY studies involving directly the measurement of E_T^{miss} (see Section 20.2).

As discussed in detail in Section 9.3.3.1, $Z \rightarrow \tau\tau$ events (with one leptonic τ-decay and one single-prong hadronic τ-decay) can be reconstructed rather accurately for events with $p_T^Z > 15$ GeV, since the expected mass resolution is about 9 GeV at low luminosity. For an integrated luminosity of 30 fb^{-1}, a sample of 3800 $Z \rightarrow \tau\tau$ signal events is expected to be reconstructed above a total background of ~200 events. This would lead to a statistical uncertainty of $\sim \pm 0.15$ GeV on the measured Z mass, and therefore the overall error would be dominated completely by the 1% uncertainty on the absolute jet energy scale, which applies in this case to the high-p_T hadronic jet from τ-decay.

Figure 12-19 shows the sensitivity of the measured Z mass, as obtained from reconstructed $\tau\tau$ pairs, to the absolute E_T^{miss} scale. A variation of $\pm$ 10% of the E_T^{miss} scale results in a shift of $\pm$ 2.5% on the measured Z mass. The E_T^{miss} scale can therefore be determined to $\pm$ 4% for an integrated luminosity of 30 fb^{-1}.

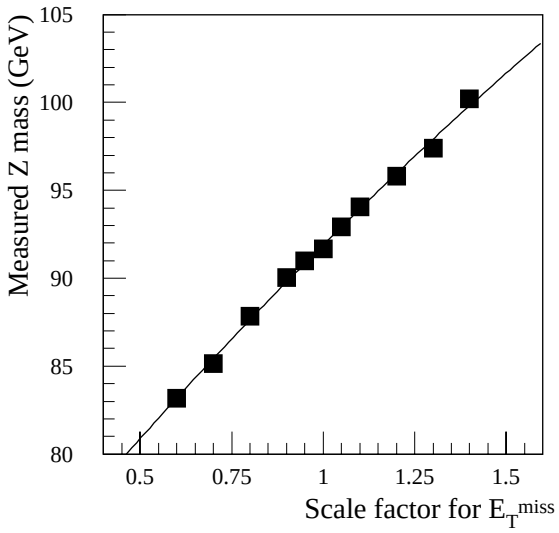

Figure 12-19 Reconstructed Z mass in the $Z \rightarrow \tau\tau$ channel as a function of the uncertainty on the E_T^{miss} scale.

12.6 Conclusions

This Chapter has described some of the prominent methods and event samples, which will be used *in situ* to evaluate the overall ATLAS mass scale to the best possible accuracy. Many of the studies reported here are based on an extrapolation of the techniques pioneered successfully at the Tevatron. Using these techniques, the experiments at the Tevatron have demonstrated that precision physics can be done at hadron colliders, in many cases on a par with that performed at e^+e^- colliders. The overall systematic uncertainties on the absolute mass scale in the Tevatron experiments have been brought to the level of 0.1% for leptons (momentum and energy measurements) and of a few percent for hadronic jet energy measurements.

The experiments at the LHC will have the added advantage of very high statistics of leptonic decays of vector bosons and of hadronic decays of W bosons from top-quark decays. Therefore, it is not unreasonable to hope that the ultimate requirements set by the physics for the systematic uncertainty on the absolute mass scale (0.02% for leptons, 0.1% for photons and 1% for hadronic jets) will be reached with the ATLAS detector.

12.7 References

12-1 CDF Collaboration, Phys. Rev. **D50** (1994) 2966 and Phys. Rev. **D 52** (1995) 4784.

12-2 D0 Collaboration, Phys. Rev. Lett. **77** (1996) 3309.

12-3 S. Haywood, 'Offline alignment and calibration of the Inner Detector', ATLAS Communication ATL-COM-INDET-99-001 (1999).

12-4 ALEPH Collaboration, ALEPH Handbook, Vol. 1 (1995).

12-5 D. Newton, H1 Internal Note, H1-8/90-145 (1990).

12-6 ATLAS Collaboration, Barrel Toroid Technical Design Report, ATLAS TDR 7, CERN/LHCC 97-19 (1997).

12-7 S. Snow, 'Magnetic field measurement requirements of the Inner Detector', ATLAS Internal Note ATL-INDET-97-196 (1997).

12-8 Z. Was *et al.*, Comput. Phys. Commun. **79** (1994) 291.

12-9 ATLAS Collaboration, Muon Spectrometer Technical Design Report, ATLAS TDR 10, CERN/LHCC/97-22 (1997).

12-10 L. Chevalier *et al.*, 'Test of the magnetic field reconstruction procedure with the race-track coil prototype', ATLAS Communication ATL-COM-MUON-99-012 (1999).

12-11 W. Lohmann *et al.*, 'Energy loss of muons in the energy range 1-10,000 GeV', CERN Yellow Report 85-03 (1985).

12-12 A. Henriques *et al.*, 'The muon energy losses in the tile calorimeter', ATLAS Internal Note ATL-TILE-95-068 (1995).

12-13 M. Aleksa, 'Absolute mass scale calibration using $Z \rightarrow \mu\mu$ events', ATLAS Internal Note ATL-MUON-99-001 (1999).

12-14 ATLAS Collaboration, Calorimeter Performance Technical Design Report, ATLAS TDR 1, CERN/LHCC/96-40 (1996).

12-15 P. Savard, 'The W to jet-jet and top quark mass reconstruction with the ATLAS detector', ATLAS Internal Note ATL-CAL-97-092 (1997).

12-16 D0 Collaboration, 'Determination of the absolute jet energy scale in the D0 calorimeters', Nucl. Instr. Meth. **A424** (1999) 352.

12-17 R. Mehdiyev and I. Vichou, 'Hadronic jet energy scale calibration using Z+jet events', ATLAS Communication ATL-COM-PHYS-99-054 (1999).